The Astrophysical Journal, 884:155 (7pp), 2019 October 20 https://doi.org/10.3847/1538-4357/ab43cb

Radiative Association of Atomic and Ionic Carbon

James F. Babb[1], R. T. Smyth[1,2], and B. M. McLaughlin[1,2]
[1] Center for Astrophysics | Harvard & Smithsonian, 60 Garden Street, MS 14, Cambridge, MA 02138, USA; jbabb@cfa.harvard.edu, rsmyth41@qub.ac.uk, bmclaughlin899@btinternet.com
[2] Centre for Theoretical Atomic, Molecular, and Optical Physics, School of Mathematics & Physics Queen's University of Belfast, Belfast BT7 1NN, UK
Received 2019 July 19; revised 2019 August 12; accepted 2019 September 9; published 2019 October 22

Abstract

We present calculated cross sections and rate coefficients for the formation of the dicarbon cation (C_2^+) by the radiative association process in collisions of a $C(^3P)$ atom and a $C^+(^2P^o)$ ion. Molecular structure calculations for a number of low-lying doublet and quartet states of C_2^+ are used to obtain the potential energy surfaces and transition dipole moments coupling the states of interest, substantially increasing the available molecular data for C_2^+. Using a quantum-mechanical method, we explore a number of allowed transitions and determine those contributing to the radiative association process. The calculations extend the available data for this process down to the temperature of 100 K, where the rate coefficient is found to be about 2×10^{-18} cm^3 s^{-1}. We provide analytical fits suitable for incorporation into astrochemical reaction databases.

Unified Astronomy Thesaurus concepts: Molecular physics (2058); Molecule formation (2076); Laboratory astrophysics (2004)

1. Introduction

The dicarbon cation C_2^+ is an important molecule in astrochemistry, as it is one of the species participating in hydrocarbon chemistry in, for example, interstellar clouds (Solomon & Klemperer 1972) and photon-dominated regions (Guzmán et al. 2015). In environments with hydrogen the dication is rapidly consumed, but it is of interest to securely characterize C_2^+ formation mechanisms as the subsequent production of larger molecules C_2H^+, $C_2H_2^+$, ... will depend on the available C_2^+.

In the present paper, we consider the formation of the dicarbon cation (C_2^+) by the radiative association process in collisions of a carbon atom and a carbon ion,

$$C(^3P) + C^+(^2P^o) \rightarrow C_2^+ + h\nu. \quad (1)$$

The process in Equation (1) is a mechanism for dicarbon cation formation, which is viable in astrochemical environments because of the applicability of two-body kinetics and because of the abundance of carbon. (Another, more recent, application is to carbon plasma chemistry can be found in Hirooka et al. (2014)). We note—we will discuss the chemistry in more detail below—that in typical astrophysical applications with relatively abundant hydrogen (in atomic and molecular form) the radiative reaction (Equation (1)) will generally be outpaced by the ionic reactions such as (Solomon & Klemperer 1972) $CH + C^+ \rightarrow C_2^+ + H$ (Federman & Huntress 1989; Guzmán et al. 2015) or $CH^+ + C \rightarrow C_2^+ + H$ (Chabot et al. 2013; Rampino et al. 2016) and Equation (1) is likely to be a minor process. Nevertheless, there is one previous calculation of Equation (1) that was carried out to a lowest temperature of 300 K, and which is listed in astrochemical reaction databases for applications below this temperature. To remove the uncertainty for astrochemical applications, it is necessary to calculate the rate coefficient at lower temperatures. In the present paper, we compute cross sections and rate coefficients for Equation (1), and provide a new calculation of the process valid down to 100 K. We find that the rate coefficient is larger for $100 < T < 300$ K than the values assumed in astrochemical databases.

The theory of the formation of diatomic species by radiative association is generally established. A recent review summarizes the theoretical methodologies and lists 73 diatomic species[3] for which calculations have been carried out (Nyman et al. 2015). There is, however, only one previous calculation for C_2^+ (Andreazza & Singh 1997), and that calculation does not extend below 300 K. (The Rice–Ramsperger–Kassel–Marcus (RRKM) theory applied to radiative association of C^+ and C_n for $n = 1, \ldots, 8$ yielded a value of zero for the rate coefficient of process in Equation (1) at 30 K, but the theory was focused on the polyatomic case.)

In a molecular description of the collisions that describe Equation (1), there are numerous possible approach channels and transitions leading to C_2^+ and the theoretical treatment of Equation (1) becomes quite complicated, as we will show. The rate coefficients for Equation (1) were calculated by Andreazza & Singh (1997) using a semi-classical description of the collisions in which the atom and ion approach in the quartet $B\ ^4\Sigma_u^-$ state, yielding a rate coefficient of about 3×10^{-18} cm^3 s^{-1} at 300 K. In this paper, we will show by calculating the cross sections using a quantum-mechanical method with improved molecular data for C_2^+ that the most significant channels are those in which the colliding atom and ion approach in molecular doublet states.

We present calculations for a number of molecular states of C_2^+, cross sections and rate coefficients for the process in Equation (1), discuss the present rate coefficients and the earlier determination, and consider in more detail the potential significance of Equation (1).

[3] We remark, somewhat tangentially, that there are also listed five polyatomic species, not including, for example, a recent calculation for the sodium ion and the hydrogen molecule (Burdakova et al. 2019).

2. Molecular Structure

Potential energies correlating to $C(^3P)$ and $C^+(^2P^o)$ were calculated by Petrongolo et al. (1981), Rosmus et al. (1986), Bruna & Wright (1992), Ballance & McLaughlin (2001), and Shi et al. (2013). There are several experimental studies of band spectra including Maier & Rösslein (1988), Boudjarane et al. (1995), and Tarsitano et al. (2004), and calculations of transition dipole moment (TDM) functions (Rosmus et al. 1986). As far as we know, no new TDM calculations have appeared since Rosmus et al. (1986), yet for the present study we will require a larger set. Therefore, we calculated a number of molecular potential energies and corresponding TDMs substantially increasing the available data for C_2^+.

The potential energy curves (PECs) and TDMs are calculated for a set of low-lying doublet and quartet electronic states that enter into the radiative association calculations. We treat the molecular states formed by the approach of $C(^3P)$ with $C^+(^2P^o)$ within an MRCI+Q approximation: a state-averaged (SA) complete-active-space-self-consistent-field (SA-CASSCF) approach, followed by multi-reference configuration interaction (MRCI) calculations, together with the Davidson correction (MRCI+Q) (Helgaker et al. 2000), is used. The SA-CASSCF method is used as the reference wave function for the MRCI calculations. The basis sets used in the present work are the augmented correlation consistent polarized core valence quintuplet (aug-cc-pcV5Z (ACV5Z)) Gaussian basis sets, which were used in our recent work on the dicarbon molecule (Babb et al. 2019) and were found to give an excellent representation of the states as the molecule dissociated.

All the PEC and TDM calculations for C_2^+ were performed with the quantum chemistry program package MOLPRO 2015.1 (Werner et al. 2015), running on parallel architectures. For molecules with degenerate symmetry, an Abelian subgroup is required to be used in MOLPRO. Thus, for $C^+(^2P^o)$ with $D_{\infty h}$ symmetry, it will be substituted by D_{2h} symmetry with the order of irreducible representations being (A_g, B_{3g}, B_{2g}, B_{1g}, B_{1u}, B_{2u}, B_{3u}, A_u). When the symmetry is reduced from $D_{\infty h}$ to D_{2h} (Herzberg 1950), the correlating relationships are $\sigma_g \rightarrow a_g$, $\sigma_u \rightarrow a_u$, $\pi_g \rightarrow (b_{2g}, b_{3g})$, $\pi_u \rightarrow (b_{2u}, b_{3u})$, $\delta_g \rightarrow (a_g, b_{1g})$, and $\delta_u \rightarrow (a_u, b_{1u})$.

To take account of short-range interactions, we employed the nonrelativistic SA-CASSCF/MRCI method available within the MOLPRO (Werner et al. 2012, 2015) quantum chemistry suite of codes. For the dicarbon cation, molecular orbitals (MOs) are put into the active space, including ($3a_g$, $1b_{3u}$, $1b_{2u}$, $0b_{1g}$, $3b_{1u}$, $1b_{2g}$, $1b_{3g}$, $0a_u$), symmetry MOs. The MOs for the MRCI procedure were obtained using the SA-CASCSF method, for doublet and quartet spin symmetries. The averaging process was carried out on the two lowest states of the symmetries: (A_g, B_{3u}, B_{1g}, B_{1u}) and the lowest states of the symmetries; (B_{2u}, B_{3g}, B_{2g} and A_u). This gives an accurate representation of the doublet and quartet states.

There are 24 molecular electronic states formed from $C(^3P)$ and $C^+(^2P^o)$, namely, $^{2,4}\Sigma^+_{g,u}$, $^{2,4}\Sigma^-_{g,u}(2)$, $^{2,4}\Pi_{g,u}(2)$, $^{2,4}\Delta_{g,u}$ (Chiu 1973; Shi et al. 2013); however, we do not consider the $2^2\Sigma^-_u$, $2^2\Sigma^-_g$, $1\ ^4\Pi_u$, $2\ ^4\Sigma^-_u$, $1\ ^4\Sigma^+_g$, $2\ ^4\Pi_u$, $1\ ^4\Delta_g$ and $2\ ^4\Sigma^-_g$ states, because they are repulsive (Shi et al. 2013) and will not be important for process in Equation (1).

PECs and TDMs as functions of internuclear distance R were calculated over the range $1.5 \leqslant R \leqslant 20$ Bohr for the 16 states listed in Table 1. In Figure 1, we present the calculated quartet PECs. In Figure 2, we present the calculated doublet PECs along with the $X\ ^4\Sigma^-_g$ PEC included for reference.

Table 1
Theoretical T_e Values (units of cm^{-1}) for the 16 States Considered in the Present Work

State	Present[a]	Other[b]
$X\ ^4\Sigma^-_g$	0	0
$a\ ^2\Pi_u$	4417	4590.09
$A\ ^4\Pi_g$	9399	9597.8
$b\ ^2\Delta_g$	10027	9943.30
$c\ ^2\Sigma^-_g$	12295	12179.74
$d\ ^2\Sigma^+_g$	13281	13505.81
$2\ ^2\Pi_u$	15238	15366.74
$B\ ^4\Sigma^-_u$	19624	19767.42
$f\ ^2\Pi_g$	22332	22618.62
$g\ ^2\Sigma^+_u$	26433	26797.85
$1\ ^4\Delta_u$	28151	28425.26
$1\ ^4\Sigma^+_u$	28273	28859.38
$1\ ^2\Sigma^-_u$	30053	30174.91
$1\ ^2\Delta_u$	33942	34221.58
$2\ ^2\Pi_g$	40767	36448.37[c]
$2\ ^4\Pi_g$	39987	40271.62

Notes. In column 2, the values of the term energies T_e are listed for the potential energies fit to Equation (2) relative to the minimum of the $X^4\Sigma^-_g$ potential energy; column 3 gives the MRCI+Q/CV+DK+56 values from (Shi et al. 2013).
[a] Present calculations.
[b] From Shi et al. (2013) MRCI+Q/CV+DK+56.
[c] The value of the second well for the $f\ ^2\Pi_g$ state in the present calculation is 36262 cm^{-1}, in agreement with the single well 36448.37 cm^{-1} given by Shi et al. (2013). See the text for a discussion.

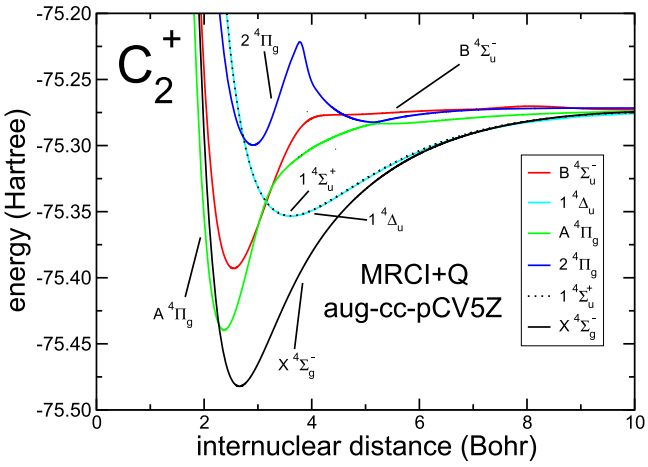

Figure 1. Calculated quartet molecular states of the C_2^+ cation as a function of internuclear distance R. We note that the $1^4\Sigma^+_u$ and the $1\ ^4\Delta_u$ states are almost degenerate in energy.

For $R \geqslant 20$ Bohr, the PECs were fit to the long-range form

$$V(R) = \frac{C_3}{R^3} - \frac{\alpha_d(\mathrm{C})}{2R^4}, \qquad (2)$$

where C_3/R^3 is the electric charge–atomic-quadrupole interaction potential energy (Gentry & Giese 1977) and $\alpha_d(\mathrm{C})$ is the static electric dipole polarizability of carbon (Miller & Kelly 1972; Das & Thakkar 1998) for each state. We utilized the $\alpha_d(\mathrm{C})$ values calculated by Das & Thakkar (1998) with the

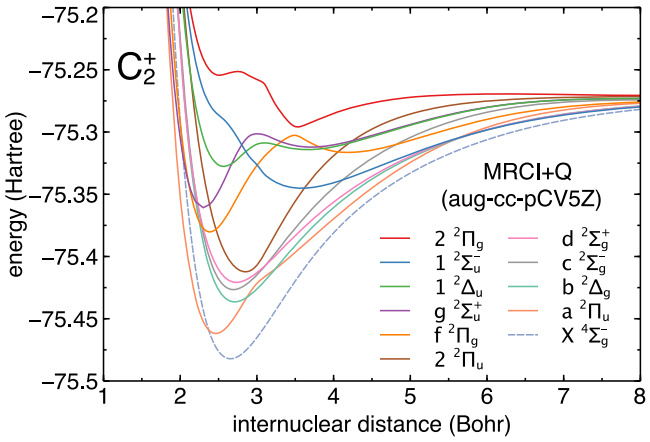

Figure 2. Calculated doublet molecular states of C_2^+ that were investigated in our cross-section calculations, as a function of internuclear distance R, with the $X^4\Sigma_g^-$ ground state indicated. In the index the states are listed in order of decreasing energy at $R = 2.6\,a_0$ starting from the left column: 2 $^2\Pi_g$, ..., 2 $^2\Pi_u$, d $^2\Sigma_g^+$, ..., X $^4\Sigma_g^-$.

finite field method and a coupled cluster CCSD(T) approach for atomic carbon in the $M_L = 0, \pm 1$ states. For example, we used $C_3 = -0.775$ and $\alpha_d(\mathrm{C}) = 12.4$ for the $X^4\Sigma_g^-$, $A^4\Pi_g$, $1^4\Delta_u$, $a^2\Pi_u$, $b^2\Delta_g$, $c^2\Sigma_g^-$, and f $^2\Pi_g$ states, and we used C_3=1.55 and $\alpha_d(\mathrm{C}) = 10.3$ for the $B^4\Sigma_u^-$, $2^4\Pi_g$, $2^2\Pi_u$, and $2^2\Pi_g$ states. For $R \leqslant 1.5$, a short-range interaction potential of the form $\exp(AR)$ was fitted to the ab initio potential curves.

The resulting T_e values measured with respect to the minimum of the $X^4\Sigma_g^-$ state are given in Table 1. We also list the values of T_e from the recent MRCI+Q/CV+DK+56 calculations of Shi et al. (2013). (Comprehensive tabulations of calculations by earlier workers (and some experimental data) were given by Shi et al. 2013.) For T_e, there is generally very good agreement (within 300 cm^{-1}) between our calculations and those of Shi et al. (2013), which also include relativistic (Douglas-Kroll effective Hamiltonian) effects and which were obtained using extrapolation procedures to account for energy dependencies on basis sets. For example, we find $T_e = 19624\ \mathrm{cm}^{-1}$ for the $B^4\Sigma_u^-$ state, in very good agreement with the experimental value of $19652.2 \pm 0.4\ \mathrm{cm}^{-1}$ (Celii & Maier 1990), while Shi et al. (2013) find an MRCI+Q/CV value of 19718.80 cm^{-1} and an MRCI+Q/CV+DK+56 value[4] of $19767.42\ \mathrm{cm}^{-1}$. For the $c^2\Sigma_g^-$ state, we find $T_e = 12295\ \mathrm{cm}^{-1}$, to be compared with calculations by Shi et al. (2013), listing an MRCI+Q/CV value of 12221.88 cm^{-1} and a CV+DK value of 12213.98 cm^{-1} (their Table 3) and an MRCI+Q/CV+DK+56 value of 12179.74 cm^{-1} (their Table 5). Similarly, for the $a^2\Pi_u$ state, we find $T_e = 4417\ \mathrm{cm}^{-1}$, while (Shi et al. 2013) find an MRCI+Q/CV+DK+56 value of 4590.09 cm^{-1}. In the case of the 2 $^2\Pi_g$ state, we find two wells with, respectively, $T_e = 40767$ and 36262 cm^{-1}, whereas Shi et al. (2013) list only a single well of depth $T_e = 36448.37\ \mathrm{cm}^{-1}$. A close comparison of Shi et al. (2013, Figure 1) and Figure 2 reveals that Shi et al. (2013) plot (and

[4] Shi et al. (2013) declare that "no other theoretical T_e is closer to the measurements" than theirs. While our value is closer to the experiment than theirs, without a detailed convergence study, our close agreement with the experiment may be coincidental. They also state "no other theoretical R_e result is superior to (theirs) in quality when compared with the measurements." We obtain the same value of $R_e = 2.55\ a_0$.

Table 2
Molecular Transitions of the Dicarbon Cation Investigated in This Work Listed in Order of Decreasing Contribution to the Total Cross Section

Initial State	to	Final State
f $^2\Pi_g$	→	a $^2\Pi_u$
2 $^2\Pi_g$	→	a $^2\Pi_u$
B $^4\Sigma_u^-$	→	X $^4\Sigma_g^-$
b $^2\Delta_g$	→	a $^2\Pi_u$
f $^2\Pi_g$	→	2 $^2\Pi_u$
2 $^2\Pi_g$	→	2 $^2\Pi_u$
1 $^2\Sigma_u^-$	→	f $^2\Pi_g$
c $^2\Sigma_g^-$	→	a $^2\Pi_u$
B $^4\Sigma_u^-$	→	A $^4\Pi_g$
2 $^2\Pi_u$	→	c $^2\Sigma_g^-$
2 $^4\Pi_g$	→	1 $^4\Sigma_u^+$
2 $^4\Pi_g$	→	1 $^4\Delta_u$
1 $^2\Delta_u$	→	f $^2\Pi_g$
2 $^4\Pi_g$	→	B $^4\Sigma_u^-$

list wells) corresponding to *diabatic* potential curves for the states of $^2\Pi_g$ symmetry, giving a single well for the 2 $^2\Pi_g$ PEC. In the adiabatic approximation, which we utilize, the f $^2\Pi_g$ and 2 $^2\Pi_g$ PECs do not cross (Herzberg 1950), and the f $^2\Pi_g$ PEC "turns over" as it approaches the 2 $^2\Pi_g$ state with increasing R yielding a second well. The avoided crossings in the present calculations between the f $^2\Pi_g$ and 2 $^2\Pi_g$ states and between the 2 $^2\Pi_u$ and 1 $^2\Pi_u$ states are in good agreement with earlier work (Petrongolo et al. 1981; Ballance & McLaughlin 2001). The accuracy of the present PECs is suitable for the present calculations of the radiative association process.

There are numerous allowed electric dipole transitions within the manifold of electronic states calculated here and listed in Table 1 (Herzberg 1950). The radiative association cross sections arise from spontaneous transitions between the vibrational continuum of the initial electronic state and a bound vibrational state of the final electronic state and depend roughly on the third power of the electronic transition energies and the square of the TDMs. Thus, we will investigate in further detail only the allowed transitions where the electronic transition energies and TDMs are comparatively large. In anticipation of the cross-section calculations presented in the next section, Table 2 gives a list of the transitions investigated here for the radiative association proccess.

Since the dominant configurations change as C_2^+ dissociates —as highlighted in the early MRDCI work of Petrongolo et al. (1981), the valence-CI calculations of Ballance & McLaughlin (2001) and in more recent elaborate MRCI+Q calculations of Shi et al. (2013)—only the initial and final molecular states are listed.

For the quartet electronic states, we selected the transitions B $^4\Sigma_u^-$–X $^4\Sigma_g^-$, B $^4\Sigma_u^-$–A $^4\Pi_g$, and B $^4\Sigma_u^-$–2 $^4\Pi_g$, with our calculated TDMs shown in Figure 3, and the 2 $^4\Pi_g$–1 $^4\Sigma_u^+$, 2 $^4\Pi_g$–1 $^4\Delta_u$, 1 $^4\Sigma_u^+$–A $^4\Pi_g$, and 1 $^4\Delta_u$–A $^4\Pi_g$ transitions, with our calculated TDMs shown in Figure 4. The B $^4\Sigma_u^-$–X $^4\Sigma_g^-$ TDM agrees with the calculations of Rosmus et al. (1986), which was given over the range $2 < R < 3.2\ a_0$. For the doublet electronic states we selected the f $^2\Pi_g$–a $^2\Pi_u$, $2^2\Pi_g$–$2^2\Pi_u$, $2^2\Pi_g$–a $^2\Pi_u$, and f $^2\Pi_g$–2 $^2\Pi_u$ transitions, where our calculated TDMs are shown in Figure 5, the c $^2\Sigma_g^-$–a $^2\Pi_u$,

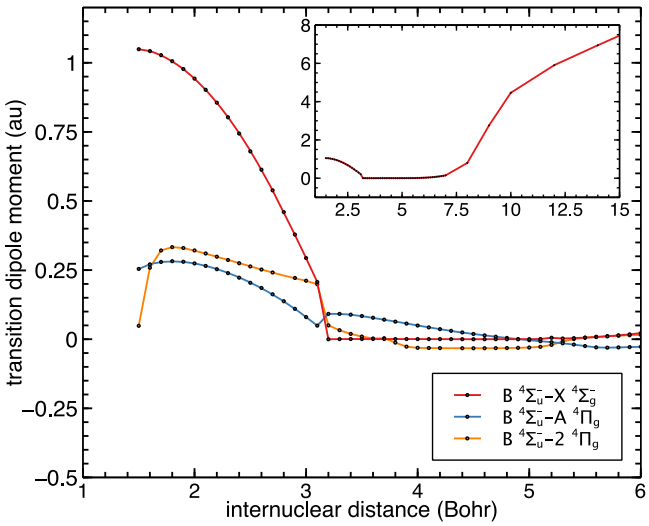

Figure 3. Transition dipole moments for quartet transitions involving the $B\ ^4\Sigma_u^-$ state as functions of internuclear distance R: $B\ ^4\Sigma_u^-$–$X\ ^4\Sigma_g^-$, $B\ ^4\Sigma_u^-$–$A\ ^4\Pi_g$, and $B\ ^4\Sigma_u^-$–$2\ ^4\Pi_g$. The inset shows that the $B\ ^4\Sigma_u^-$–$X\ ^4\Sigma_g^-$ function approaches $\frac{1}{2}R$ for large R.

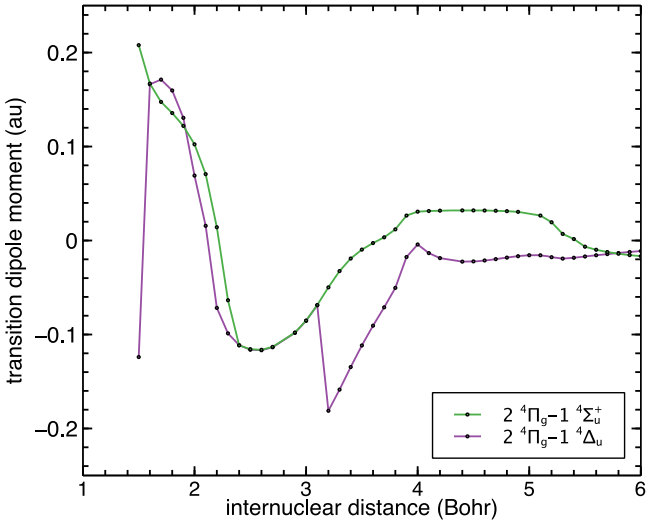

Figure 4. Transition dipole moments for quartet transitions as a functions of internuclear distance R: 2 $^4\Pi_g$–1 $^4\Sigma_u^+$, and 2 $^4\Pi_g$–1 $^4\Delta_u$.

2 $^2\Pi_u$–$c\ ^2\Sigma_g^-$, and $b\ ^2\Delta_g$–$a\ ^2\Pi_u$ transitions, where our calculated TDMs are shown in Figure 6, and the $f\ ^2\Pi_g$–$1\ ^2\Delta_g$ and $f\ ^2\Pi_g$–$1\ ^2\Sigma_g^-$ transitions, where our calculated TDMs are shown in Figure 7. Our calculated value of the $f\ ^2\Pi_g$–$a\ ^2\Pi_u$ TDM at $R = 2.4$ is 0.06, in atomic units, which agrees with the estimate calculated at this single value of R by Rosmus et al. (1986).

In general, the quartet and doublet TDMs are well-behaved at the lower and upper limits of the ranges of R for which they are calculated. However, we note that for the quartet TDMs, Figures 3 and 4, there are sharp jumps around $R = 3.2$. We attribute this to changes in the dominant configurations in the electronic wave functions around the four-way intersection of the $A\ ^4\Pi_g$, $B\ ^4\Sigma_u^-$, $1\ ^4\Delta_u$, and $1^4\Sigma_u^+$ PECs, see Figure 1. Moreover, the $1^4\Sigma_u^+$ and $1\ ^4\Delta_u$ states are nearly degenerate (Petrongolo et al. 1981; Shi et al. 2013) and the TDMs for 2 $^4\Pi_g$–1 $^4\Sigma_u^+$ and 2 $^4\Pi_g$–1 $^4\Delta_u$ become equal over the range $2.4 < R < 3.1$. In the case of the doublet TDMs, rapid variation around $R = 2.9$ in the functions involving the $a\ ^2\Pi_u$

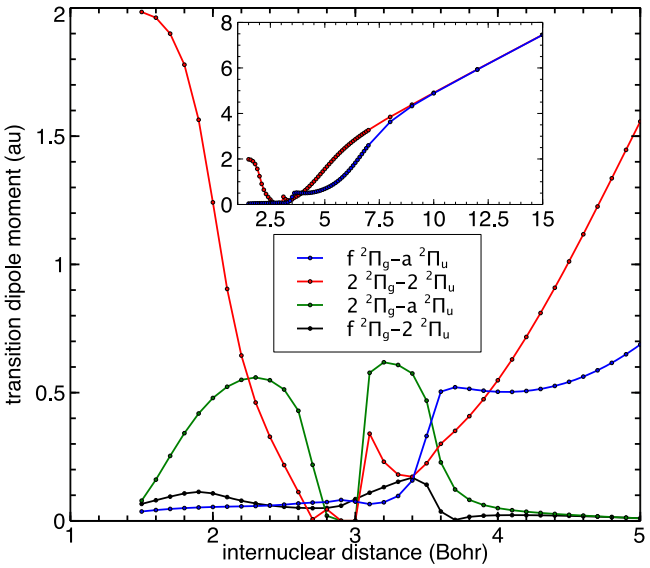

Figure 5. Transition dipole moments between $^2\Pi_g$ and $^2\Pi_u$ states as a function of internuclear distance R: $f\ ^2\Pi_g$–$a\ ^2\Pi_u$, $2\ ^2\Pi_g$–$2^2\Pi_u$, $2\ ^2\Pi_g$–$a\ ^2\Pi_u$, and $f\ ^2\Pi_g$–$2^2\Pi_u$. The inset shows that the 2 $^2\Pi_g$–$a\ ^2\Pi_u$ and $f\ ^2\Pi_g$–$a\ ^2\Pi_u$ functions approach $\frac{1}{2}R$ for large R.

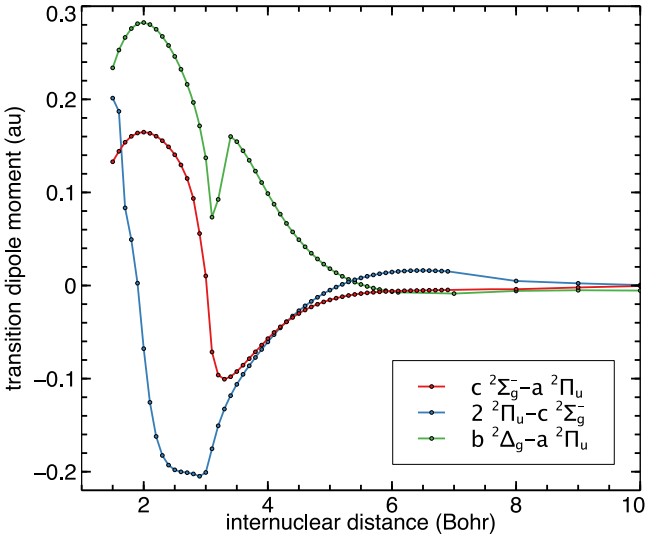

Figure 6. Transition dipole moments as a function of internuclear distance R between $^2\Pi_u$ states and the $c\ ^2\Sigma_g^-$ state and for the $b^2\Delta_g$–$a\ ^2\Pi_u$ transition.

and 2 $^2\Pi_u$ states, Figures 5 and 6, reflects the avoided crossing between the PECs where the dominant configuration of the $a\ ^2\Pi_u$ state changes (Petrongolo et al. 1981; Ballance & McLaughlin 2001). A more detailed analysis of the electronic state configurations and their effect on the TDMs should be carried out for spectroscopic applications, such as for calculations of band oscillator strengths. Such an analysis is unnecessary for our purposes, because, as we will show, the most important factors leading to significant radiative association cross sections are the lack of a barrier in the PEC and a significant TDM at large R. The $f\ ^2\Pi_g$ entrance channel lacks a barrier and the TDMs for the $B\ ^4\Sigma_u^-$–$X\ ^4\Sigma_g^-$, $f\ ^2\Pi_g$–$a\ ^2\Pi_u$, and $2^2\Pi_g$–$2^2\Pi_u$ transitions approach $R/2$ for large R, as shown in the insets of Figures 3 and 5, similarly to the A–X TDM of O_2^+ (Wetmore et al. 1984).

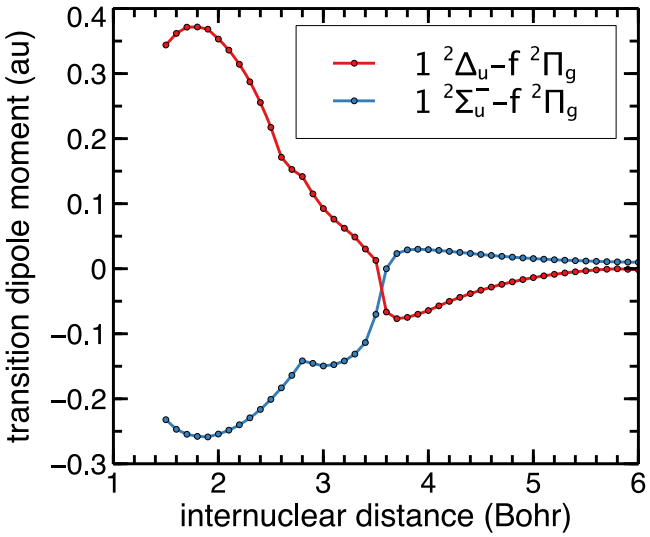

Figure 7. Transition dipole moments for $f\ ^2\Pi_g$–$1\ ^2\Delta_u$ and $f\ ^2\Pi_g$–$1\ ^2\Sigma_u^-$ as a function of internuclear distance R.

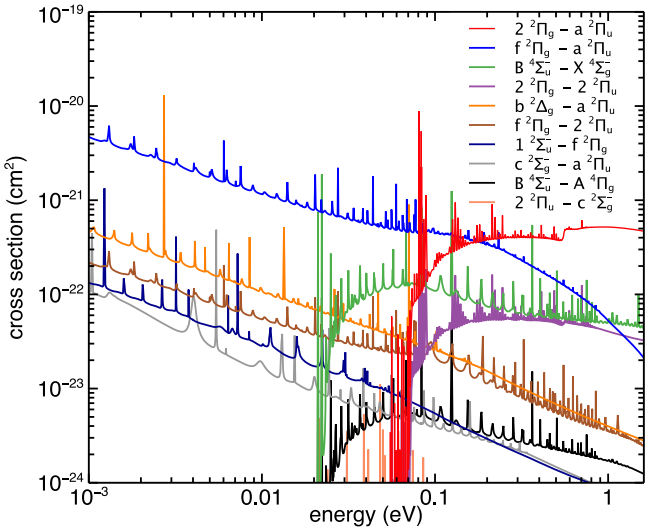

Figure 8. Cross sections (in units of cm^2) as functions of the collisional energy (in units of eV) for doublet and quartet transitions. The weight factors are set to unity in this plot.

The TDMs were fit to the form $1/R^4$, for $R \geqslant 20$, except for the $B^4\Sigma_u^-$–$X^4\Sigma_g^-$, $f^2\Pi_g$–$a^2\Pi_u$, and $2^2\Pi_g$–$2^2\Pi_u$ transitions which were fit to $R/2$ at large nuclear separations.

3. Cross Sections

The radiative association cross sections for each transition listed in Table 2 contributing to the process in Equation (1) were calculated for ^{12}C nuclei as a function of the collision energy using the quantum-mechanical formalism, which was previously applied to like-atom-ion radiative association for species without nuclear spin; for He and He$^+$ (Stancil et al. 1993; Augustovičová et al. 2013) and for O and O$^+$ (Babb et al. 1994).

From the 24 molecular electronic states formed from C(^3P) and C$^+$($^2P^o$) there are 72 possible approach channels considering that due to the absence of nuclear spin only half of the possible lambda doubling levels are populated for $\Lambda = 1$ or 2. Thus the weight factor appearing in the cross section for an entrance collision channel labeled by i is $P_i = \frac{1}{72}(2S_i + 1)$. Because the collisional cross sections will be mainly due to partial waves with $N \gg 1$, we approximate $J = N$ and use Hund's case (b) coupling, where N is the rotational quantum number, J is the total angular momentum $|\boldsymbol{N} + \boldsymbol{S}|$, and S is the total electronic spin, as in our previous work on radiative association of O and O (Babb & Dalgarno 1995). The reduced mass μ is 10937.35 in units of the electron mass. As discussed in Section 2, the PECs and TDM functions utilized were fit to appropriate long-range forms. The cross sections were evaluated using the methods detailed in Babb et al. (2019). For collisions in the $B\ ^4\Sigma_u^-$ entrance channel only odd partial waves were treated, while for the $1\ ^4\Sigma_u^+$ and $c\ ^2\Sigma_g^-$ entrance channels only even partial waves were treated.

The calculated cross sections are shown in Figure 8. We do not plot the cross sections for the $2\ ^2\Pi_u$–$c\ ^2\Sigma_g^-$, $2\ ^4\Pi_g$–$1\ ^4\Sigma_u^+$, $2\ ^4\Pi_g$–$1\ ^4\Delta_u$, $1\ ^2\Delta_u$–$f\ ^2\Pi_g$, and $2\ ^4\Pi_g$–$B\ ^4\Sigma_u^-$, transitions, which were found to be insignificant. Note that we also explored the $1\ ^4\Sigma_u^+$–$A\ ^4\Pi_g$ and $1\ ^4\Delta_u$–$A\ ^4\Pi_u$ transitions and found that the TDMs are comparable in magnitude to those shown in Figure 4.Therefore because the transition energies are comparable to the states shown in that figure, we expect the cross sections to be insignificant.

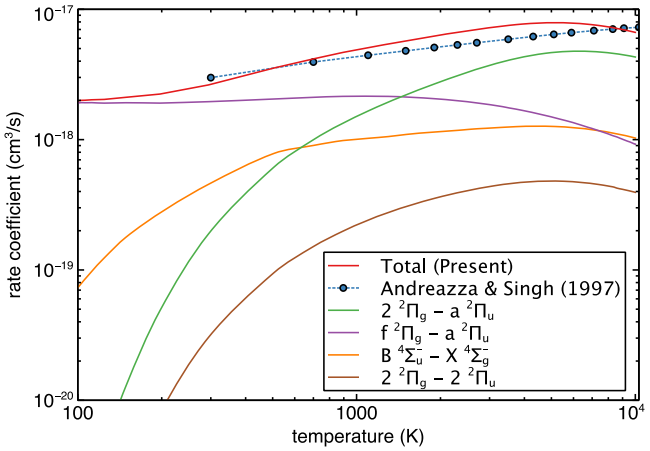

Figure 9. Rate coefficients (in units of cm^3 s^{-1}) as as functions of temperature (in units of K) for the dominant channels contributing to the radiative association association process (1). The rate coefficients for the four transitions and the sum are plotted in comparison to the calculations of Andreazza & Singh (1997).

4. Rate Coefficients

The rate coefficients were calculated by averaging the cross sections over a Maxwellian velocity distribution. The dominant entrance channels were found to be the doublet $f\ ^2\Pi_g$ and $2\ ^2\Pi_g$ states and the quartet $B\ ^4\Sigma_u^-$ state. The dominant transitions are $f\ ^2\Pi_g$–$a\ ^2\Pi_u$, $2\ ^2\Pi_g$–$2\ ^2\Pi_u$, $2\ ^2\Pi_g$–$a\ ^2\Pi_u$, and $B\ ^4\Sigma_u^-$–$X\ ^4\Sigma_g^-$. The rate coefficients for these four transitions and the total rate coefficients are shown in Figure 9 with the rate coefficients for the $B^4\Sigma_u^-$–$X^4\Sigma_g^-$ transition from Andreazza & Singh (1997).

The agreement between our total rate coefficients and those from Andreazza & Singh (1997) is good but appears to be accidental. Andreazza & Singh (1997) selected the $B^4\Sigma_u^-$–$X^4\Sigma_g^-$ transition based on a careful analysis of available TDM data from the literature. In particular, they determined

that doublet transitions would not contribute significantly compared to their predictions for the strengths of the $B^4\Sigma_u^- - X^4\Sigma_g^-$ transition. Andreazza & Singh (1997) considered the $f\ ^2\Pi_g - a\ ^2\Pi_u$ transition but estimated that it was insignificant based on the relatively small TDM value at $R = 2.4$ calculated by Rosmus et al. (1986). As discussed in Section 2, our calculated TDM is in agreement with the estimate given by Rosmus et al. (1986); however, as illustrated in Figure 5 we find that the TDM of the $f\ ^2\Pi_g - a\ ^2\Pi_u$ transition grows linearly with internuclear distance and consequently this is the most significant contribution to the process Equation (1) at the lowest energies because there is no barrier in the $f\ ^2\Pi_g$ approach channel. In contrast, while the $2\ ^2\Pi_g$ and $B\ ^4\Sigma_u^-$ approach channels have barriers and will not contribute at the lowest energies, for sufficient collisional energies the $2\ ^2\Pi_g - 2\ ^2\Pi_u$ and $B\ ^4\Sigma_u^- - X\ ^4\Sigma_g^-$ transitions become dominant.

The rate coefficients for the $B\ ^4\Sigma_u^- - X\ ^4\Sigma_g^-$ transition calculated by Andreazza & Singh (1997) increase slowly over the temperature range from 300 to 14,700 K, varying from about 3×10^{-18} cm^3 s^{-1} at 300 K to 7.6×10^{-18} cm^3 s^{-1} at 14,700 K. In the present calculations, there is a barrier of about 0.023 eV (effective kinetic temperature of 270 K) at about $R = 9\ a_0$, in the $B\ ^4\Sigma_u^-$ state. Thus, as is evident in Figure 8, the cross sections for the $B\ ^4\Sigma_u^- - X\ ^4\Sigma_g^-$ and $B\ ^4\Sigma_u^- - A\ ^4\Pi_g$ transitions rapidly diminish for collisional energies below 0.023 eV and these transitions will be inefficient at temperatures below about 300 K, in marked contrast to the calculations of Andreazza & Singh (1997), which do not show a rapid decrease of the $B\ ^4\Sigma_u^- - X\ ^4\Sigma_g^-$ transition rate coefficient below 1000 K. Therefore, any apparent agreement between the total rate coefficient obtained here and the calculations of Andreazza & Singh (1997), certainly for temperatures below 1000 K, must be accidental. Because of the similarity between the $2\ ^2\Pi_g - a\ ^2\Pi_u$ and $B\ ^4\Sigma_u^- - X\ ^4\Sigma_g^-$ TDMs and because the well depths of the $a\ ^2\Pi_u$ and the $X\ ^4\Sigma_g^-$ PECs are comparable the earlier calculations of Andreazza & Singh (1997) are in good agreement with the present results, though the identifications of the dominant formation channels for the formation of C_2^+ via process (1) differ.

The total calculated rate coefficient $\alpha(T)$ is fit to better than 11% by the expression

$$\alpha(T) = a + bT + cT^2 + dT^3\ (\mathrm{cm^3\ s^{-1}}), \quad 100 < T < 10{,}000\ \mathrm{K}, \tag{3}$$

with $a = 1.9038 \times 10^{-18}$, $b = 2.9628 \times 10^{-21}$, $c = -4.4649 \times 10^{-25}$, and $d = 1.9827 \times 10^{-29}$.

5. Discussion

We find that the rate coefficient for process (1) is about 2×10^{-18} cm^3 s^{-1} at 100 K. It is important to note that the only prior existing calculation (Andreazza & Singh 1997) is valid for temperatures greater than 300 K. As we showed, the calculation of Andreazza & Singh (1997) agrees fortuitously with our calculation over the range $300 < T < 10{,}000$ K and they provided the fit

$$\alpha_{\mathrm{AS97}}(T) = 4.01 \times 10^{-18}(T/300)^{0.17} \times \exp(-101.52/T)\ \mathrm{cm^3\ s^{-1}}. \tag{4}$$

In the context of astrochemical models, the fit provided by Andreazza & Singh (1997), which was limited to $300 < T < 14{,}700$ K, is implemented in astrochemical databases that are applied to temperatures below 300 K. Moreover, applying the fit function from Andreazza & Singh (1997), for example, (incorrectly) to 100 K yields a rate coefficient that is a factor of two lower with an exponential decrease for $T < 100$ K. The fit, Equation (4), is listed as applicable for $10 < T < 41{,}000$ K in the UMIST RATE12 file,[5] and was used, for example, in the photon-dominated region code comparison study[6] with the same temperature validity listed (Röllig et al. 2007). The present rate coefficients are fit, to within 4% by the function

$$\alpha_{\mathrm{low}}(T) \approx 2.55 \times 10^{-18}(T/300)^{0.26}\ \mathrm{cm^3\ s^{-1}} \quad 100 < T < 300\ \mathrm{K}. \tag{5}$$

Based on the trend of the $f\ ^2\Pi_g - a\ ^2\Pi_u$ cross section with decreasing collision energy, see Figure 8, and estimating the rate coefficient using $\alpha \sim \langle \sigma(E)v \rangle$, where $v = 2E/\mu$ with μ the reduced mass, we can expect that the rate coefficient will be no greater than 2×10^{-18} cm^3 s^{-1} at 10 K, though a detailed calculation considering the fine structure of $C(^3P)$ and $C^+(^2P^o)$ should be performed (the fine structure splitting of $C^+(^2P^o)$ is about 63.4 cm^{-1} or ~91 K). The calculated rate coefficients for (1) are small, and the process will certainly be unimportant when hydrogen is present. Nevertheless, we conclude that the present rate coefficient will lead to an enhancement in C_2^+ production, generally speaking, in astrochemical models, compared to using the fit (4), which is invalid for $T < 300$ K.

6. Conclusions

We calculated the rate coefficients for the formation of C_2^+ by radiative association of $C(^3P)$ and $C^+(^2P^o)$; process (1). We substantially added to the available molecular data on C_2^+ by calculating a large set of PECs and TDMs. We found that the dominant approach channels contributing to process (1) are the doublet $f\ ^2\Pi_g$ and $2\ ^2\Pi_g$ states and that the quartet $B\ ^4\Sigma_u^-$ approach channel is of lesser importance. The rate coefficient for process (1) should not decrease exponentially as temperature decreases because there is no barrier in the dominant $f\ ^2\Pi_g$ entrance channel. As a consequence, the present rate coefficients will lead to enhanced production of C_2^+ in astrophysical models, though the net impact may be insignificant when hydrogen is present.

We thank Dr. Romane Le Gal for helpful discussions. This work was supported by a Smithsonian Scholarly Studies grant. ITAMP is supported in part by NSF grant No. PHY-1521560. B.M.Mc.L. acknowledges support by the ITAMP visitor's program, by the University of Georgia at Athens for the award of an adjunct professorship, and by Queen's University Belfast for a visiting research fellowship (VRF). We thank Captain Thomas J. Lavery, USN, Ret., for his constructive comments that enhanced the quality of this manuscript. The authors acknowledge this research used grants of computing time at the National Energy Research Scientific Computing Centre (NERSC), which is supported by the Office of Science of the U.S. Department of Energy (DOE) under Contract No. DE-AC02-05CH11231. The authors gratefully acknowledge the

[5] http://udfa.ajmarkwick.net/index.php?species=46, accessed 2019 August 4.

[6] Reaction rate file `rate99_edited_incl_crp.dat` available at https://zeus.ph1.uni-koeln.de/site/pdr-comparison/benchmark.htm, accessed 2019 August 4.

Gauss Centre for Supercomputing e.V. (www.Gauss-center.eu) for funding this project by providing computing time on the GCS Supercomputer HAZEL HEN at Höchstleistungsrechenzentrum Stuttgart (www.hlrs.de).

Software: MOLPRO (v. 2015.1) (Werner et al. 2015).

ORCID iDs

James F. Babb https://orcid.org/0000-0002-3883-9501
R. T. Smyth https://orcid.org/0000-0002-4359-1408
B. M. McLaughlin https://orcid.org/0000-0002-5917-0763

References

Andreazza, C. M., & Singh, P. D. 1997, MNRAS, 287, 287
Augustovičová, L., Špirko, V., Kraemer, W. P., & Soldán, P. 2013, A&A, 553, A42
Babb, J., Fan, Z., & Dalgarno, A. 1994, JQSRT, 52, 161
Babb, J. F., & Dalgarno, A. 1995, PhRvA, 51, 3021
Babb, J. F., Smyth, R. T., & McLaughlin, B. M. 2019, ApJ, 876, 38
Ballance, C. P., & McLaughlin, B. M. 2001, JPhB, 34, 1201
Boudjarane, K., Carré, M., & Larzillière, M. 1995, CPL, 243, 571
Bruna, P. J., & Wright, J. S. 1992, J. Phys. Chem., 96, 1630
Burdakova, D., Nyman, G., & Stoecklin, T. 2019, MNRAS, 485, 5874
Celii, F., & Maier, J. 1990, CPL, 166, 517
Chabot, M., Béroff, K., Gratier, P., Jallat, A., & Wakelam, V. 2013, ApJ, 771, 90
Chiu, Y.-N. 1973, JChPh, 58, 722
Das, A. K., & Thakkar, A. J. 1998, JPhB, 31, 2215
Federman, S. R., & Huntress, W. T., Jr. 1989, ApJ, 338, 140
Gentry, W. R., & Giese, C. F. 1977, JChPh, 67, 2355
Guzmán, V. V., Pety, J., Goicoechea, J. R., et al. 2015, ApJL, 800, L33
Helgaker, T., Jørgensen, P., & Olsen, J. 2000, Molecular Electronic-Structure Theory (New York: Wiley)
Herzberg, G. 1950, Spectra of Diatomic Molecules (New York: Van Nostrand)
Hirooka, Y., Sato, H., Ishihara, K., Yabuuchi, T., & Tanaka, K. 2014, NucFu, 54, 022003
Maier, J. P., & Rösslein, M. 1988, JChPh, 88, 4614
Miller, J. H., & Kelly, H. P. 1972, PhRvA, 5, 516
Nyman, G., Gustafsson, M., & Antipov, S. V. 2015, IRPC, 34, 385
Petrongolo, C., Bruna, P. J., Peyerimhoff, S. D., & Buenker, R. J. 1981, JChPh, 74, 4594
Rampino, S., Pastore, M., Garcia, E., Pacifici, L., & Laganà, A. 2016, MNRAS, 460, 2368
Röllig, M., Abel, N. P., Bell, T., et al. 2007, A&A, 467, 187
Rosmus, P., Werner, H.-J., Reinsch, E.-A., & Larsson, M. 1986, J. Electron. Spectrosc., 41, 289
Shi, D., Niu, X., Sun, J., & Zhu, Z. 2013, JPCA, 117, 2020
Solomon, P. M., & Klemperer, W. 1972, ApJ, 178, 389
Stancil, P. C., Babb, J. F., & Dalgarno, A. 1993, ApJ, 414, 672
Tarsitano, C. G., Neese, C. F., & Oka, T. 2004, JChPh, 121, 6290
Werner, H.-J., Knowles, P. J., Knizia, G., et al. 2015, MOLPRO, version 2015.1, a Package of ab initio Programs, http://www.molpro.net
Werner, H.-J., Knowles, P. J., Knizia, G., Manby, F. R., & Schütz, M. 2012, WIREs Comput. Mol. Sci., 2, 242
Wetmore, R. W., Fox, J. L., & Dalgarno, A. 1984, P&SS, 32, 1111